NMR Solution Structure of a DNA Dodecamer Duplex Containing a *cis*-Diammineplatinum(II) d(GpG) Intrastrand Cross-Link, the Major Adduct of the Anticancer Drug Cisplatin†

Andrew Gelasco and Stephen J. Lippard*

Department of Chemistry, Massachusetts Institute of Technology, Cambridge, Massachusetts 02139

Received December 30, 1997; Revised Manuscript Received March 27, 1998

ABSTRACT: The structure of the DNA duplex dodecamer, d(CCTCTG*G*TCTCC·GGAGACCAGAGG), containing the cisplatin d(GpG) 1,2-intrastrand cross-link at the position denoted by asterisks, was determined in solution by high-resolution 2D NMR spectroscopy and restrained molecular dynamics refinement. The *cis*-[Pt(NH_3)$_2${d(GpG-N7(1),N7(2))}] lesion causes the adjacent guanine bases to roll toward one another by 49°, leading to an overall helix bend angle of 78°. These features are more exaggerated than those observed in the X-ray crystal structure determined for the same platinated duplex [Takahara et al. (1995) *Nature 377*, 649−652]. A common property of the solution and crystal structures is the widening and flattening of the minor groove opposite the platinum adduct, affording geometric parameters resembling those found in A-form DNA. This deformation is especially noteworthy for the solution structure because its sugar puckers are primarily those of B-form DNA. The unwinding of the helix at the site of platination is 25°. The curvature and shape of the platinated duplex are remarkably similar to those observed in DNA duplexes complexed by the HMG-domain proteins SRY and LEF-1. The structure reveals how cisplatin binding alters DNA in such a manner as to facilitate HMG-domain protein recognition.

The anticancer drug cisplatin[1] binds to DNA affording mainly intrastrand d(GpG) and d(ApG) cross-links (*1*, *2*). Other adducts include 1,3-d(GNG) intrastrand and d(G)-d(N) interstrand cross-links (*1*). The formation of these different adducts causes varying degrees of duplex bending and unwinding as determined by gel electrophoresis studies (*3*, *4*). The structural consequences of cisplatin 1,2-intrastrand DNA cross-links are of particular interest because their presence in cancer patients correlates with a positive response to treatment with the drug (*5*). Studies from our laboratory and others have determined that these adducts are recognized by proteins containing one or more high-mobility group (HMG) domains (*6*−*9*). Proteins in this family shield the 1,2-intrastrand d(GpG) and d(ApG) adducts from excision repair both in vitro (*10*, *11*) and in vivo (*12*). Understanding in detail the structural distortions of duplex DNA caused by cisplatin 1,2-intrastrand cross-links should reveal features responsible for their recognition and binding by HMG-domain proteins.

An X-ray crystal structure determination of *cis*-[Pt(NH_3)$_2$-{d(pGpG-N7(1),N7(2))}] indicated that the *cis*-diammineplatinum(II) moiety binds to the N7 atoms of the two guanine rings, which are oriented in a head-to-head manner and significantly destacked, the dihedral angle between the purine base planes being 81° (*13*, *14*). The solution structure of d(GpG) bound similarly to *cis*-{Pt(NH_3)(4-aminoTEMPO)}$^{2+}$, a paramagnetic analogue of *cis*-{Pt(NH_3)$_2$}$^{2+}$, has similar features as revealed by a combination of diamagnetic and paramagnetic NMR spectra in combination with molecular modeling (*15*).

More recently, the crystal structure of a duplex dodecamer d(5′-$C_1C_2T_3C_4T_5G_6$*G_7*$T_8C_9T_{10}C_{11}C_{12}$-3′)·d(5′-$G_{13}G_{14}A_{15}$-$G_{16}A_{17}C_{18}C_{19}A_{20}G_{21}A_{22}G_{23}G_{24}$-3′), **1**, where G*G* represents the 1,2-intrastrand cisplatin adduct, was solved to 2.6 Å resolution (*16*, *17*). This work provided the first X-ray structure determination of a duplex DNA containing the major cisplatin lesion and revealed many interesting features. A very shallow roll angle of only 26° toward the major groove was induced by platinum binding at the G*G* step, resulting in considerable strain at the Pt−N7 bonds. In particular, the Pt atom was displaced from the plane of each guanine base by approximately 1 Å. The platinum lesion compacted the major groove and unwound the duplex, giving rise to a widened and flattened minor groove, similar to that observed in A-form DNA. The duplex also contained an A-form/B-form junction situated just to the 3′ side of the platinum adduct. An analysis of the unit cell packing revealed end-to-end and end-to-groove interactions between the platinated duplexes. We were therefore interested in determining the extent to which these duplex deformations observed in the solid state would be retained in solution.

† This work was supported by Grant CA34992 from the National Cancer Institute. A.G. is supported by a postdoctoral fellowship from the National Cancer Institute.

* To whom correspondence should be addressed.

[1] Abbreviations: cisplatin or *cis*-DDP, *cis*-diamminedichloroplatinum(II); HMG, high-mobility group; NMR, nuclear magnetic resonance; NOESY, nuclear Overhauser effect spectroscopy; SRY, sex-determining region Y protein; LEF-1, lymphoid enhancer binding factor 1; CPG, controlled pore glass; ddH_2O, distilled, deionized water; d_5-TSP, 1,1,1-trisilyl-2,3-dideuteriopropionic acid; NaP_i, sodium phosphate; HPLC, high-performance liquid chromatography; MWCO, molecular weight cutoff; SCUBA, acquisition delay for underwater peak recovery; PECOSY, purged exclusive correlated spectroscopy; TOCSY, totally correlated spectroscopy; NOE, nuclear Overhauser effect; FID, free induction decay; RMSD, root-mean-squared deviation.

S0006-2960(97)03176-0 CCC: $15.00
Published on Web 06/11/1998

NMR studies have been carried out on duplex DNAs containing a variety of platinum lesions. Recently, solution structures were reported for two different self-complementary duplex decamer DNAs containing (dG)(dG) *inter*strand cross-links (*18*, *19*). The overall features of the two structures were nearly identical, with the cross-link positioning the platinum atom in the minor groove and producing an 80° unwinding at the site of platination. The complementary cytosines were displaced from the helix. These structures enforce a highly localized change in handedness of the duplex from right-handed B- to left-handed Z-form DNA, bending it toward the minor groove by ~45° at the interstrand cross-link.

Early attempts to elucidate the solution structure of the cisplatin 1,2-*intra*strand cross-link in double-stranded DNA by NMR methods indicated that the duplex formed a kink toward the major groove at the platinum coordination site (*20*, *21*). The structures were determined with the aid of molecular mechanics and dynamics calculations to build models consistent with observed NMR data, but they were not restrained by NOESY-derived distances. The kink was estimated to be ~60° and the remainder of the helix was in an undistorted B-form. More recently, the NMR solution structure of the octameric duplex d(CCTG*G*TCC)·d(GGACCAGG), **2**, was reported (*22*). This short duplex was bent by ~58° toward the major groove and unwound by ~21°, leading to a slightly widened minor groove. These overall features are similar to those observed for the crystal structure of the platinated dodecamer duplex **1** (*17*) and the study afforded the first high-resolution insight into cisplatin binding to its major site in double-stranded DNA in solution.

In the present work, we have examined the solution structure of the platinated dodecamer **1**. We chose this compound for detailed analysis in order to probe the structural consequences of the major cisplatin adduct over at least one turn of DNA helix and to provide the desired comparison between the solution and solid state for cisplatin interacting with the same DNA sequence. The observed structural features, determined by NMR spectroscopy and restrained molecular dynamics, are compared to those in the crystal (*17*) and in the NMR-derived structure of the duplex octamer (*22*). The geometry is further compared to the DNA duplexes in complexes with the HMG-domain proteins SRY (*23*) and LEF-1 (*24*), affording insight into how cisplatin-modified DNA can be recognized by this class of proteins.

EXPERIMENTAL PROCEDURES

Materials. *cis*-Diamminedichloroplatinum(II) was obtained as a gift from Johnson Matthey AESAR/Alfa Co. Reagents for preparing DNA were used as received from Cruachem. In HPLC experiments, buffer A is 25 mM NH_4-OAc, pH 6.0, and 10% acetonitrile, and buffer B is buffer A plus 1 M NaCl. Both 99.9% and 99.996% D_2O and d_4-TSP were purchased from Cambridge Isotope Laboratories. Ultrapure Na_2HPO_4, NaH_2PO_4, 30% NH_4OH, and NaCl were purchased from American Bioanalytical Co.

Synthesis and Purification of Oligonucleotides. The dodecamer oligonucleotides d(CCTCTGGTCTCC) (**1**ts-un) and d(GGAGACCAGAGG) (**1**bs) were prepared by the phosphoramidite method on a Cruachem PS250 DNA synthesizer equipped with a 15 μmol column. The crude oligomers were cleaved from the CPG column and were deprotected by treatment with concentrated NH_4OH (aq). The solutions of **1**ts-un and **1**bs were lyophilized to dryness, redissolved in ddH_2O, and passed through a Sephadex G25 size exclusion column. The oligomer **1**ts-un was converted to the sodium salt on a Dowex cation exchange column and then made 10 mM in NaP_i (pH 6.0). The activated form of cisplatin, *cis*-$[Pt(NH_3)_2(H_2O)_2]^{2+}$, was prepared by allowing *cis*-DDP to react with 1.97 equiv of $AgNO_3$ in ddH_2O overnight in the dark. The white AgCl suspension was separated by centrifugation, and the solution was decanted and recentrifuged. The resulting supernatant was then added to the **1**ts solution at a ratio of 1.3 Pt/strand and allowed to incubate for 15 h at 37 °C. The platinated and unmodified strands were purified by anion-exchange HPLC on a Dionex Nucleopac PA-100 semi-prep chromatographic column connected to a Waters 600E system controller and Waters 484 tunable absorbance detector with a 80% A/20% B → 65% A/35% B 30 min NaCl gradient. The HPLC-purified fractions were extensively desalted by dialysis against deionized water (Spectrum Spectra/Por 7 tubing, 1000 MWCO) and lyophilized to dryness. The oligomers were finally purified by G25 size exclusion gel filtration.

The platinum/oligonucleotide ratio was determined to be 1:1 by atomic absorption spectrophotometry on a Varian 1475 graphite furnace AA instrument, with detection at 266 nm. Platinum concentrations were standardized against a Pt AA standard diluted from a stock solution obtained from Aldrich Chemical Co.

NMR samples were prepared by adding a 1 mM solution of the platinated oligomer to a 1 mM solution of the complementary strand to an approximate 1:1 ratio in diluted NMR buffer, 100 mM NaCl, 10 mM NaP_i, pH 6.9. The DNA was annealed by cooling from 70 °C to ambient temperature, and the extent of duplex formation verified by ion-exchange HPLC. The resulting solution was lyophilized to dryness and dissolved in either D_2O or H_2O to an approximate concentration of 3 mM. DNA melting curves were obtained on both the platinated and unmodified oligomers at approximate duplex concentrations of 2 μM in a buffer containing 100 mM NaCl, 10 mM NaP_i, pH 6.9. Data were collected on an AVIV UV−visible scanning spectrometer connected to a temperature bath regulated to ±0.1 °C.

NMR Spectroscopy of Platinated Duplex DNA. The purified duplex d(CCTCTG*G*TCTCC)·d(GGAGACCAGAGG) was annealed by slow cooling from 70 °C in 100 mM NaCl and 10 mM NaP_i, pH 6.9, at an approximate concentration of 3 mM. Deuterated d_5-TSP was added to a concentration of 0.25 mM (1.8 mM ^1H). The sample was dried three times from 99.6% D_2O and finally dissolved to afford a concentration of 3.2 mM in duplex in 99.996% atom D_2O. The final sample was again annealed by slow cooling from 70 °C in the NMR tube.

NMR Data Collection and Processing. NMR spectra were measured at 15 ± 0.1 °C with the carrier frequency set coincident with the residual HDO signal and referenced relative to TSP at 0.0 ppm. Data were collected at both 750 and 600 MHz and processed with the Felix 95.0 NMR software from Biosym Technologies.

Two identical samples of **1** were prepared. A series of NOESY spectra with mixing times of 70, 110, 150, 200,

and 300 ms was collected in D_2O on a custom-built 750 MHz spectrometer at the Francis Bitter Magnet Laboratory (FBML) at MIT. Presaturation of the residual HDO signal was accomplished by using a 2 s pulse during the pre-acquisition delay. A SCUBA − 60 ms recovery step during the NOESY pulse sequence was used to allow observation of the H3′ proton signals near the water resonance. The preacquisition delay was empirically chosen to be 10 μs, the resulting probe recovery eliminating the need for linear phase correction of the processed data. For each spectrum, a total of 512 increments containing 4096 complex points were collected with a spectral width of 8000 Hz, with each FID representing an average of 32 transients containing a total recycle delay of 4 s. Additional spectra were measured in D_2O including a PECOSY spectrum collected at 750 MHz and 50 and 70 ms TOCSY spectra measured at 600 MHz in order to confirm sugar proton chemical shifts assignments and the deoxyribose sugar puckers.

Two NOESY spectra of **1** were recorded in a 90%/10% H_2O/D_2O solution at 110 and 200 ms on the 750 MHz spectrometer. Water suppression was carried out by using the WATERGATE gradient pulse sequence prior to the NOESY data collection. Residual water signals were removed by convolution difference solvent suppression, as implemented in Felix 95.0, during data processing.

All 2D NMR spectra collected at FBML were processed in Felix 95.0. The t2 data were processed after a background correction and $\pi/2$ shifted sine-squared apodization of the data in the time domain. The series of processed spectra were baseline corrected by using the automatic baseline correction routine in Felix 95.0. The first point in the t1 dimension of each spectrum was linearly predicted back from the first 64 data points to compensate for the need for linear phase correction in the indirectly detected dimension. The 512 data increments were linearly predicted forward to 2048 points, $\pi/2$ shifted sine-squared apodized, and zero filled to 4096 points before Fourier transformation and automatic baseline correction. The use of the $\pi/2$ shifted sine-squared bell function was critical for these spectra, since it provided for accurate integrations in both dimensions; this set of spectra was used for quantitative NOE measurements.

Spectra collected on the 600 MHz instrument contained 4096 points in each FID in t2 and 512 experiments in t1, with spectral widths of 7002 Hz in each dimension. Each FID was collected as an average of 16 transients with a total recycle delay of 4.5 s. The carrier offset was set coincident with the HDO peak in each spectrum. The residual water signal was suppressed with a 2 s presaturation pulse during preacquisition. All spectra were processed in a similar manner with the Felix 95.0 software package by utilizing slight line broadening (1.5 Hz) in the t2 dimension and a $\pi/2$ shifted sine-squared weighting function over 512 points in t1 and zero filled to 4096 points prior to Fourier transformation.

Model Building. Starting models for the structure refinement were prepared in Quanta 4.1 (Molecular Simulations Inc., Waltham, MA). Initial A-form and B-form duplex models were prepared and modified by docking the *cis*-diammineplatinum(II) residue to the N7 atoms of G6* and G7*. Molecular structure files for each duplex type were prepared by running models through XPLOR 3.1 (*25*) using the all atom force field containing explicit hydrogen bond potentials. Force constants and charges for the diammineplatinum(II) fragment and the bound guanine bases were modified from a molecular mechanics calculation by Herman et al., (*21*), and those found in the XPLOR 3.1 parameter files (*25*). Initial models were energy minimized without NOE restraints using the Powell minimization routine in XPLOR 3.1 to obtain idealized geometry for bond lengths and angles prior to any refinement procedures.

RESULTS

NMR Spectroscopy. The two-dimensional NOESY spectra processed in Felix 95.0 were imported into in NMRCompass 2.5 (Molecular Simulations Inc). Assignments of the H8/H6 base and H1′ sugar protons were made through analysis of the 110 and 300 ms NOESY spectra by established methods (*26*, *27*). Figure 1 shows duplicate contour plots of the H1′/H5-to-H8/H6/H2 region of the 300 ms NOESY spectrum. The sequential connectivity from *n*H8/H6 to *n*H1′ and from *n*H1′ to (*n* + 1)H8/H6 for C1 to C12 in the platinated top strand and for G13 to G24 in the complementary bottom strand is observed for the duplex **1**, as would be expected for right-handed duplex DNA. There is some variation in the intensities of the cross-peaks at the ends of the complementary strand and those corresponding to the bases T5, G6*, and G7* at the site of platination. Additionally, NOE cross-peaks are observed for some of the internucleotide cytosine H5 protons to the H6/H8 base protons. These cross-peaks are labeled in the figure as peaks A−D. Deoxyadenosine H2 protons can be assigned based on cross-peaks to interstrand and internucleotide H1′ sugar protons and are indicated by peak labels E−I in Figure 1.

The H3′ and H2′ and H2″ sugar protons were assigned by using an analogous NOESY walk between the base and sugar protons. Figure 2 shows the contour plot of the H3′ to aromatic region of the 200 ms NOESY spectrum in D_2O. The connectivities between the base and sugar protons for each nucleotide and the flanking nucleotides are shown in Figure 2 for both the platinated (Figure 2A) and unmodified (Figure 2B) strands. A similar variation in intensities around the site of platination is observed for the H3′-to-H8/H6 walk, as was observed in the H1′ walk, and even at 750 MHz there still remains significant overlap between some cross-peaks. A contour plot of the H2′/H2″/thymidine Me-to-aromatic region from a 70 ms NOESY spectrum is shown in Figure S1 (Supporting Information). A combination of the 70, 150, and 200 ms NOESY spectra, the PECOSY spectrum, and the TOCSY spectra collected at 15 °C was used to complete and confirm the assignment of the sugar protons including the H4′ and most of the H5′/H5″ protons. Table 1 compiles the chemical shifts of all of the nonexchangeable protons for the platinated duplex. The stereospecific assignment has been made for the H2′/H2″ protons but not for all of the H5′/H5″ protons.

Important exchangeable protons in **1** were assigned by analysis of the 200 ms NOESY spectrum collected at 15 °C in 90% H_2O/10% D_2O. Figure S2 shows the cytosine amino and adenosine H2 proton-to-cytosine proton H5 regions and the corresponding aromatic-to-imino region of the 200 ms spectrum. The imino-to-imino contour plot is contained in Figure S3. The cross-peaks from the imino protons to deoxyadenosine H2 protons and cytosine C4 amino protons

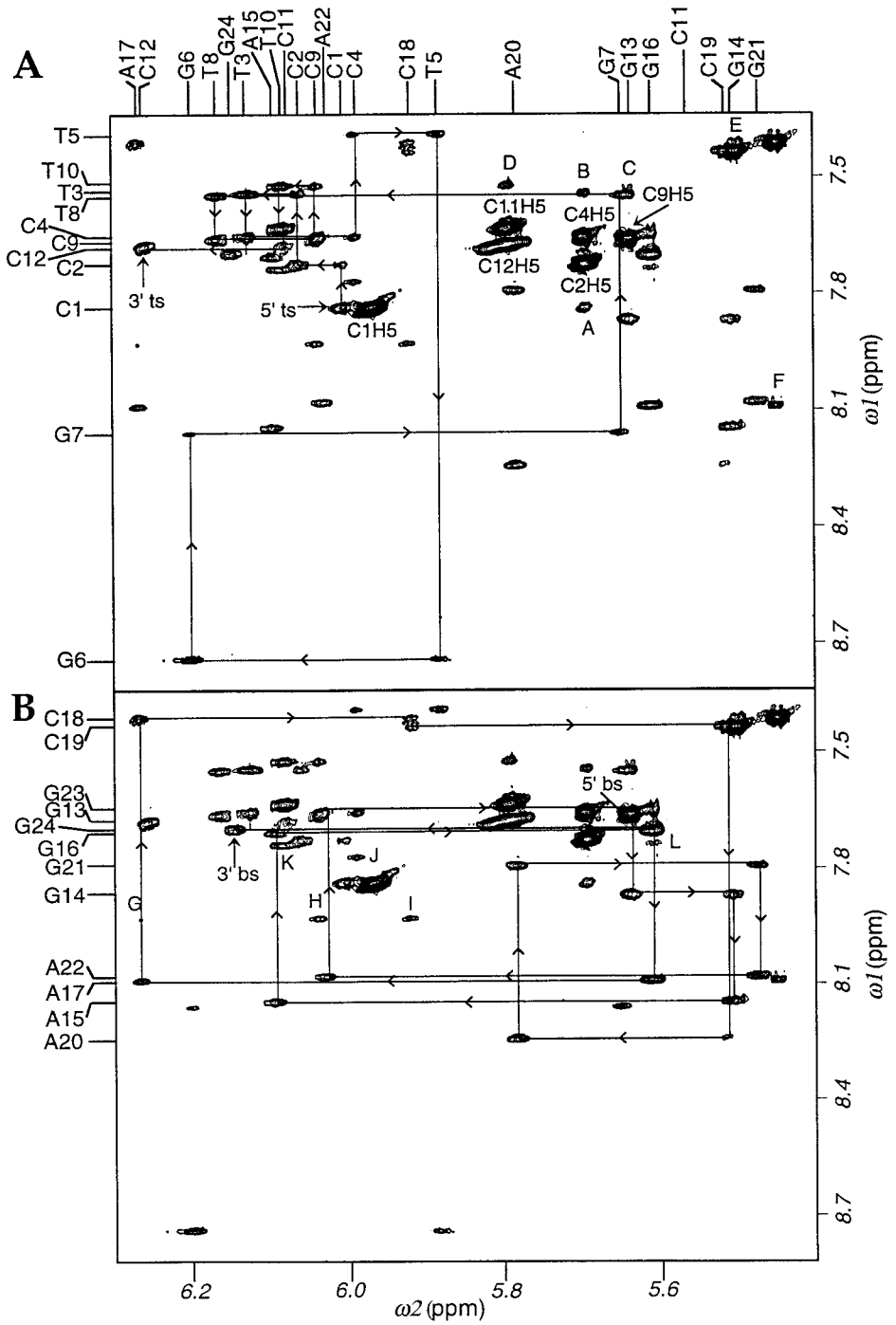

FIGURE 1: Duplicate contour plots of the H1′/H5 to aromatic region (H8/H6/H2) of the 300 ms NOESY spectrum. The sequential NOESY walk is shown in the top plot (A) for the platinated top strand (**1**ts) and in the bottom plot (B) for the unmodified bottom strand (**1**bs). The cross-peaks labeled A−E in panel A are from internucleotide H5−H6 NOEs: A, C1H6−C2H5; B, T3H6−C4H5; C, T8H6−C9H5; D, T10H6−C11H6; E, C19H6−C18H5. The cross-peaks labeled F−J in panel B are from internucleotide and interstrand NOEs to AH2 protons: F, A17H2−C19H1′; G, A17H2−C9H1′; H, A17H2−C18H1′; I, A22H2−C4H1′; J, A15H2−C11H1′.

are labeled and their assignments indicated in the figure caption. On the basis of these assignments, nine well-resolved imino protons could be unambiguously identified. Figure S3 shows the NOESY connectivity between adjacent imino protons. These connectivities are labeled for the base pairs C2−G23 to T5−A20 and from G7*−C18 to C11−G14. The imino protons for the terminal base pairs can be observed and have been assigned using 1D and 2D spectroscopy at 4 °C, but NOEs to other protons were not observed. The imino proton of G6* is not detected, indicating that the G6*−C19 base pair is distorted with the G6* H1 proton exchanging with the solvent. The amino protons from C19 are well separated in chemical shift, indicative of their involvement in a hydrogen bond. The single G6* O6···C19 NH4 hydrogen bond was included as a distance constraint with a large error during restrained molecular dynamics. The chemical shifts for the assigned exchangeable protons are included in the compilation in Table 1.

The integrals of the assigned cross-peaks for the series of five D_2O NOESY spectra were measured in NMRCompass 2.5. The unambiguously assigned NOE integrals from the

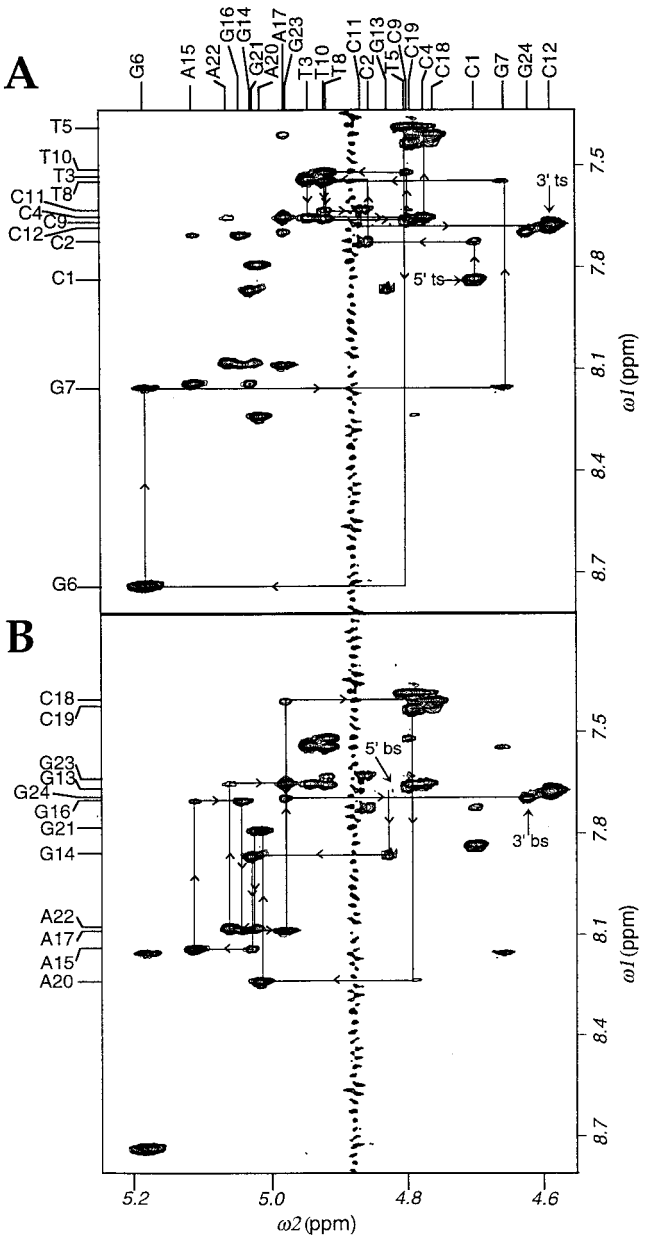

FIGURE 2: Duplicate contour plots of the aromatic-to-H3′ region of the 200 ms NOESY spectrum of **1**. The sequential connectivities of H8/H6-to-H3′ for the platinated strand is shown in panel A and for the unmodified strand in panel B.

110 ms spectrum were converted to distance constraints by using the isolated spin-pair approximation method. The distance between thymidine C6 proton and the C5 methyl group was taken as 2.9 Å and used as a calibration for proton−methyl cross-peaks; the cytosine H6−H5 distance (2.45 Å) was used to calibrate the proton−proton cross-peaks.

Structure Determination of the Cisplatin-Modified Duplex Dodecamer. The calibrated intensities calculated from the 110 ms NOESY spectrum were input into XPLOR 3.1 as distance restraints with a distance range of ±15% for $d \leq 3.5$ Å and of ±25% for $3.5 \leq d \leq 5.0$ Å. Initial energy minimized A- and B-form DNA duplex models were subjected to runs consisting of 200 cycles of distance restrained Powell minimization, 20 ps of constant temperature (300 K) simulated annealing (SA), followed by an additional 1000 cycles of Powell minimization. In addition to the 410 ^{1}H-^{1}H NOEs, explicit base-pair constraints were input as distance ranges between heavy atoms involved in hydrogen bonding. Initially, only hydrogen bonds were used in the base pairs which could be experimentally observed in 1D and 2D NMR spectra at 15 °C. Sugar puckers were input in initial refinements as explicit low-energy dihedral angles based on observed base H8/H6 proton to sugar H2′ and H3′ proton NOEs. This procedure resulted in the deoxyribose rings of G6* and C12 being input with C3′ endo conformations. All other sugar conformations were input as C2′ endo, consistent with the experimental data.

The short molecular dynamics runs with randomly assigned initial atom velocities resulted in families of structures from both the A-form and B-form starting models, which were very similar in energy and contained a small number of NOE violations. The structures all had similar overall geometries and were subjected to multiple rounds of simulated annealing, resulting in further agreement of the structures and an RMSD of 1.3 Å between averaged minimized models. NOE violations and the primary structural differences between the different duplex models occurred near the central four base pairs TG*G*T·ACCT. Longer molecular dynamics runs proved to be important for refining this highly distorted part of the duplex as well as fitting some of the weaker NOE restraints. An XPLOR refinement consisting of 180 ps of constant temperature SA with initial A-form and B-form models resulted in families of the two structures having an average overall RMSD of 1.15 Å, which can be considered to be converged.

The structures were further refined by the full relaxation matrix approach (*28*, *29*). A NMR spectrum is back-calculated in XPLOR based on a model structure. All of the 2055 intensities from the five NOESY spectra were then used as input for direct refinement against an energy penalty function determined from the difference in the observed and back-calculated NOE intensities based on the current model (*28*). An isotropic correlation time of 4.0 ns was calculated using a grid search to obtain a minimum value for the *R* factor, which was used for all relaxation matrix refinements. The refinement contained a 3 ps simulated annealing stage in which the distance restraints were reduced to zero and the relaxation weight was raised while the temperature of the refinement was lowered from 400 to 150 K. The temperature was raised to 300 K over another 1 ps. The structures were then subjected to 26 ps of constant temperature simulated annealing with the only NOE-type restraints included being hydrogen bond potentials in addition to the intensities in the relaxation matrix calculation. This type of refinement resulted in a very closely related family of structures having an average RMSD of 0.5 Å, a final average model for which is shown in Figure 3.

*Structure of the Platinated Duplex Dodecamer, **1**.* The sharp 1D ^{1}H NMR signals exhibited by **1**, together with the single set of detectable proton resonances in the 2D NOESY spectra, indicate that the duplex exists predominantly as a single structure in solution on the NMR time scale. The detection of a nearly complete set of sequential connectivities for the base H8/H6 to sugar H1′ (Figure 1), H2′/H2″ (Figure S1), and H3′ (Figure 2) protons require a stable right-handed double-helical structure. The only disruptions in connectivity occur between the G23 H1′/H3′ and G24 H8 protons and between T5 H1′/H3′ and G6* H8 protons (Figures 1 and 2).

Table 1: ^{1}H Chemical Shift Assignments (ppm) for the Duplex d(CCTCTG*G*TCTCC)·d(GGAGACCAGAGG)[a]

base	H6/H8	H5/CH_3/H2	H1′	H2′/H2″	H3′	H4′	H5′/H5″	GH1/TH3	CH4b/H4f[b]
C1	7.836	5.969	6.005	2.295/2.589	4.702	4.152	3.824/3.801		7.776/7.050
C2	7.726	5.703	6.063	2.240/2.561	4.857	4.248	4.135/4.135		8.386/7.047
T3	7.542	1.674	6.128	2.366/2.585	4.946	4.294	4.163/4.163	13.805	
C4	7.653	5.705	5.991	2.177/2.496	4.780	4.210	4.444/4.145		8.419/7.148
T5	7.388	1.738	5.882	1.398/2.431	4.807	4.081		14.390	
G6	8.742		6.203	2.579/2.755	5.185	4.276	4.312/4.207		
G7	8.159		5.647	2.298/2.594	4.665	4.235	4.119/4.119	13.189	
T8	7.548	1.308	6.167	2.339/2.581	4.920	4.302	4.199/4.199	13.960	
C9	7.655	5.696	6.041	2.184/2.573	4.802	4.199	4.086/4.086		8.432/7.064
T10	7.517	1.695	6.087	2.237/2.571	4.921	4.237	4.121/4.121	13.903	
C11	7.632	5.793	6.081	2.244/2.507	4.875	4.476			8.579/7.084
C12	7.676	5.800	6.235	2.311/2.303	4.592	4.066	4.202/4.178		8.283/7.145
G13	7.650		5.635	2.517/2.680	4.835	4.179	3.674/3.670	12.840	
G14	7.866		5.503	2.711/2.790	5.032	4.356	4.054/4.054	12.920	
A15	8.143	7.745	6.097	2.730/2.945	5.114	4.466	4.251/4.168		
G16	7.705		5.611	2.654/2.742	5.048	4.430	4.254/4.182	12.757	
A17	8.089	7.942	6.263	2.600/2.844	4.982	4.423	4.317/4.317		
C18	7.415	5.458	5.922	1.958/2.379	4.760	4.093	4.042/4.042		8.038/6.817
C19	7.437	5.512	5.518	1.889/2.288	4.795	4.046	3.957/3.957		8.440/6.828
A20	8.241	7.694	5.790	2.791/2.802	5.020	4.312	4.085/3.898		
G21	7.794		5.477	2.617/2.726	5.032	4.365	4.152/4.152	12.669	
A22	8.081	7.781	6.036	2.620/2.861	5.064	4.439	4.215/4.146		
G23	7.654		5.613	2.181/2.588	4.982	4.365	4.182/4.182	13.001	
G24	7.697		6.146	2.456/2.363	4.627	4.242	4.135/4.135	13.240	

[a] G*G* represents the site of the *cis*-diammineplatinum(II) intrastrand cross-link. [b] CH4b is the cytosine amino proton involved in hydrogen bonding in the CG base pair, CH4f is the non-hydrogen-bonded amino proton.

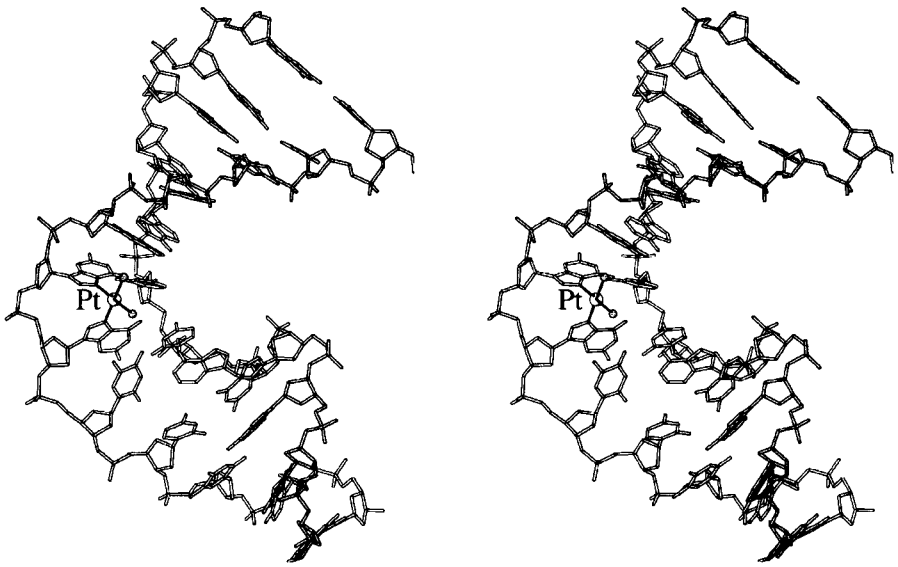

FIGURE 3: A stereoview MOLSCRIPT (*36*) plot of the final refined model of the solution structure of the platinated duplex **1**, viewed from the side. The Pt atom in the *cis*-diammineplatinum lesion is labeled. From this view, the bend in the helix and the roll at the platinated guanine bases are clearly visible.

The positions of the missing peaks are indicated by arrows in each of the NOESY spectra. The occurrence of these connectivities even at shorter mixing times (70 ms, data not shown) is consistent with all bases being oriented in an anticonformation.

The structure of the platinated dodecamer (Figure 3) is quite distorted from either of the starting A- or B-form models. We have demonstrated that the NOE constraints are sufficient to reach this converged structure from either model. The resulting duplex is primarily B-form based on sugar puckers and phosphate−phosphate distances. Only the G6* deoxyribose ring has a C3′-endo sugar pucker. This result is required by the experimental data; direct comparison of the cross-peaks in the aromatic-to-H3′ region of the 200 ms ^{1}H NOESY spectrum (Figure 2) shows qualitatively that the G6*/H8-to-/H3′ ^{1}H NOE is much more intense than all of the other cross-peaks. The other sugar puckers, including those of G7*, T5, and C12, are of the S type, having either a C2′-endo or the related C3′-exo conformation.

Although the general features, including phosphate−phosphate distances as well as sugar puckers, resemble those of B-form DNA, the structure of the platinated duplex **1** is very different. The helical base−base and base−step parameters which describe this duplex were calculated by using the program CURVES 5.1 (*30*, *31*) and are defined according to the EMBO Workshop on DNA Curvature and Bending (*32*). The binding of *cis*-diammineplatinum(II) to the N7 atoms of the adjacent guanine bases G6* and G7*

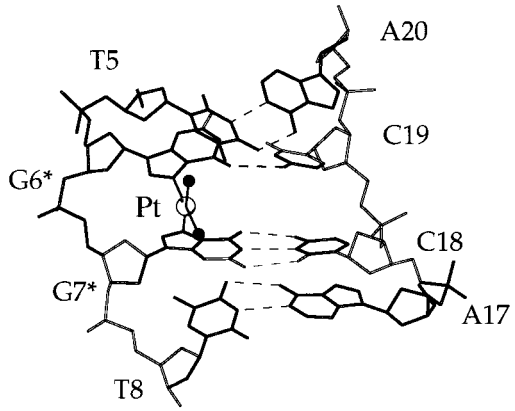

FIGURE 4: A MOLSCRIPT plot of the central four base pairs from the refined duplex structure. The unwinding of the duplex and the destacking of the T5-A20 base pair from the G6* and C19 bases are shown. Dashed lines indicate the hydrogen bonds of the base pairs, including the single C19NH4-G6*O6 hydrogen bond observed for the platinum modified guanosine.

causes a roll of 49° toward the major groove, resulting in a global bend of the double helix of ~78°. This roll and the geometric distortion at the G6*−G7* base step are required by the NMR data. In the aromatic region of the 200 ms NOESY spectrum (Figure S4), there is an intense cross-peak for the G6* H8 and G7* H8 protons. No other H8/H6-to-H8/H6 NOEs are observed for the other base steps of the duplex at this mixing time, indicating no internucleotide H8/H6 distances less than 4.5 Å.

An expanded view of the structure at the platinum-binding site is provided in Figure 4. Coordination of Pt to the N7 atoms of adjacent guanosine residues and the orientation of guanine bases in a head-to-head configuration (*13*) result in a significant NOE between the G6* and G7* H8 protons as well as their downfield chemical shifts (G6*, 8.742 ppm and G7*, 8.159 vs 7.650−7.866 for the other G H8 resonances). The G7* H8 proton chemical shift lies upfield from that of G6* H8 because of shielding by the purine ring of G6*. Coordination of these bases to platinum results in disruption of the 5′ G*C base pair. In the final structure, only the G6* O6···C19 N4 hydrogen bond remains intact, as indicated by the NMR data. In addition, the Pt atom is displaced from the planes of the each of the guanine bases by approximately 0.8 Å.

The most interesting and unexpected feature of the structure may be the deformation of the minor groove opposite the site of platination, which is quite shallow and widened, resembling the minor groove of A-form DNA. This distortion is distributed over five bases pairs, from C4−G21 through T8−A17, the minor groove being opened to 9.0−12 Å over the region and having a depth range 0.4−2.5 Å. These values may be compared to the average width of 5.7 Å and depth of 6.5 for B-form DNA, measured near the 3′ end of the duplex. The widening and flattening of the minor groove in **1** is accompanied by significant unwinding of the duplex around the site of platination, by approximately 25° starting at the T8−A17 base pair and extending to T5−A20. Figure 5 graphically depicts the variation in minor groove width for **1**.

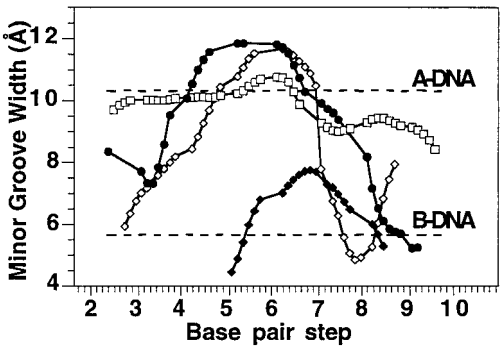

FIGURE 5: Graphical representation of the variation in minor groove width as a function of base pair step for the series of platinated duplexes described in the text. (□) Crystal structure of **1**, (●) solution structure of **1**, (◆) solution structure of **2**, (◇) solution structure of **3**.

DISCUSSION

The formation of the cisplatin 1,2-intrastrand d(G*pG*) cross-link causes significant structural deviations of DNA from the canonical B-form duplex (Figures 4 and 5). There is a significant bend of 78° toward the major groove resulting largely from the 49° guanine−guanine roll at the site of platination. These values are larger than those observed in the solid-state structure determined for this same duplex by X-ray crystallography (*17*), as discussed in more detail below. The geometry is determined primarily by NOE restraints and results directly from refinement against the data. In structural analyses of related cisplatin-modified DNAs (*21*), the geometry is fixed to be consistent with NMR data but not further constrained by the large number (400) NOEs observed here. Although the use of conventional NOE-determined distance constraints has limitations in DNA structure determination (*15*, *33*), in the present case, the bend angle and base conformations in the vicinity the platinum lesion are determined exclusively by NOEs between protons of adjacent nucleotides and the force field potential describing the *cis*-$\{Pt(NH_3)_2\}^{2+}$ adduct.

The crystal and solution structures of **1**, and the solution structure of the octameric duplex analogue **2** (*22*), all reveal that the platinum atom is displaced from the planes of the guanine rings (Table 2). This result differs from that observed in the crystal structure of the platinated dinucleotide *cis*-[$Pt(NH_3)_2${d(pG*pG*)}], in which the dihedral angle between guanine ring planes is 80° (*13*). The geometry of the *cis*-$\{Pt(NH_3)_2\}^{2+}$ moiety is much less strained in this case because the DNA fragment is short and single stranded. The 0.8 Å displacement of the platinum atom from the guanine planes in the solution structure of **1** is smaller than that observed in the crystal (~1 Å) of the same dodecamer duplex but still significantly distorted (*16*, *17*). The displacement of the Pt atom from the guanine base planes is correlated with the roll, as illustrated in Figure S6 for a series of structures containing the *cis*-[$Pt(NH_3)_2${d(pG*pG*)}] 1,2-intrastrand cross-link, and induces strain in the Pt−N7 bonds (*17*).

One possible consequence of the roll at the G*G* step and the resulting strain induced in the Pt−N7 bonds may be to labilize the platinum−guanine linkages. Such behavior is manifest at the 1,2-*intra*strand Pt cross-link in **2**, which is metastable and converts to an *inter*strand cross-link over the course of a few days (*22*). The new cross-link forms between the 5′-G* (G4) and G9, the 5′ terminal guanosine of the complementary strand. In the initially formed 1,2-intrastrand cross-linked structure, N7 of G9 is >12 Å away from the

Table 2: Selected Structural Features of Cisplatin/DNA, hSRY/DNA, and LEF-1/DNA Structures

	1 (solution structure)	**1** (crystal structure)	**2**	hSRY/DNA complex	LEF-1/DNA complex
DNA form	primarily B	A/B junction	primarily B	intermediate A/B	intermediate A/B
minor groove width/depth	9.4−12.5 Å/1.4 Å	9.5−11.0 Å/3.0 Å	4.5−7.8 Å/3.2 Å	9.4 Å	11.0 Å
avg P−P distance	6.8 Å	5.5 Å	6.8 Å	5.4 Å	6.3 Å
roll	49°	26°	42°	19°	52°
	Pt coordination	Pt coordination	Pt coordination	Ile intercalation	Met intercalation
Pt atom displacement from guanine ring planes	0.8 Å, 5′ 0.8 Å, 3′	1.3 Å, 5′ 0.8 Å, 3′	1.0 Å, 5′ 0.8 Å, 3′		
avg helical twist	27°	32°	25°	26°	32°
DNA bend	78°	39 and 55°, two independent molecules	58°		
protein/DNA bend	∼80−90°	∼80−90°	∼80−90°	∼70−80°	∼117°

platinum atom, but there is apparently enough flexibility at the ends of the duplex to facilitate the intramolecular reaction. No such rearrangement occurs with duplex **1**. NMR experiments carried out both at 15 and 20 °C over 2−8 day intervals revealed no change in spectral features or quality of the data. Moreover, duplex **1** required more than 2 weeks to form visible crystals and nearly 9 months to be of acceptable diffraction quality, during which time no apparent isomerization occurred (*17*). It is possible that the very short length and low melting temperature of duplex **2** are responsible for the reactivity of its strained Pt−N7 bonds, whereas in longer duplexes, the helix is better maintained by the four additional base pairs, resulting in a much more stable platinum lesion.

The GC base pairing at the G6*pG7* step of duplex **1** differs for the structures determined by X-ray crystallography and solution NMR spectroscopy. In the crystal structure, the base pair between G6* and C19 is fully formed, whereas the 3′ base pair between G7* and C18 is distorted. These features may be a consequence of the shallow roll between adjacent guanosines. In solution, the G6*−C19 base pair retains only one hydrogen bond; base pair G7*−C18 is normal. That the imino proton of G7* is base paired with C18 is revealed by NOESY cross-peaks between this hydrogen atom and the T8 H3 imino (Figure S3), the A17 H2 aromatic (Figure S2), and the C18 H4 amino protons (Figure S2). The more pronounced G6*pG7* roll in the solution structure would appear to be causing the disruption of the 5′ base pair. In duplex **2**, the 5′ base pair also appears to be disrupted (*22*).

One key difference between the crystal and solution structures of **1** is the greater effect of platination on the global duplex geometry manifest primarily in the large helix bend angle and extended minor groove deformation. In the crystal structure, there are eight mainly A-type base pairs, an A−B junction at T8−A17, and four mainly B-type base pairs. This geometry may be induced by crystal packing, which might limit the degree of duplex bending and unwinding. In solution, the overall structural features of roll and bend are maintained by this unwinding which spreads over five base pairs, from C4−G21 to T8−A17. This long span of duplex unwinding causes the average rise per base pair to increase by nearly 0.7 Å/residue, distorting the shape considerably from that of B-form DNA (*34*). The minor groove width is also exaggerated in this solution structure.

Figure 5 plots minor groove widths, obtained by a continuous groove measurement in CURVES 5.1 (*30*, *31*), for a series of platinated DNA structures as a function of

Scheme 1

1
$C_1\ C_2\ T_3\ C_4\ T_5\ G_6{*}\ G_7{*}\ T_8\ C_9\ T_{10}C_{11}C_{12}$
$G_{24}G_{23}A_{22}G_{21}A_{20}C_{19}\ C_{18}\ A_{17}G_{16}A_{15}G_{14}G_{13}$

2
$C_1\ C_2\ T_3\ G_4{*}\ G_5{*}\ T_6\ C_7\ T_8$
$G_{16}G_{15}A_{14}C_{13}\ C_{12}\ A_{11}G_{10}G_{10}$

3
$C_1\ T_2\ C_3\ T_4\ C_5\ G_6{*}\ G_7{*}\ T_8\ C_9\ T_{10}C_{11}$
$G_{22}A_{21}G_{20}A_{19}G_{18}C_{17}\ C_{16}\ A_{15}G_{14}A_{13}G_{12}$

base pair step. In the crystal structure of **1**, the duplex retains a primarily A-form minor groove shape over its entire length, with a slight bulge at the site of the platinum lesion. The minor groove of the platinated octamer **2**, which contains the same central four base pairs as duplex **1**, widens and then narrows as one proceeds through the platinum cross-link, but never really approaches the width of A-form DNA. The widening that does occur can probably be attributed to helix unwinding in this short duplex induced by the platinum adduct. The solution structure of an undecamer duplex, which contains a nitroxide spin-labeled platinum adduct, **3** (*33*) (Scheme 1), also has a similar but much more pronounced minor groove width variation quite similar to that observed in the present investigation. The widening of the minor groove near the site of platination is accompanied by a flattening, as described above.

Direct comparison of the solution and crystal structures of **1** obtained by superimposing the sugar−phosphate backbones reveals a remarkable similarity in global curvature of the helix. The RMSD for the non-hydrogen atoms between these two structures including all 12 base pairs and the Pt atom is 3.7 Å. The RMSD for atoms of the sugar−phosphate backbone of the eight base pairs beginning at the 5′ end of the platinated strand is 2.7 Å. Views of this superposition are shown in Figure 6. From the side, the helix backbones are clearly seen to be quite similar (Figure 6A). A view down the 5′ ends (Figure 6B) reveals a hole reminiscent of A-DNA, discussed in more detail elsewhere (*16*, *17*). Although 23 of the 24 nucleotides have C2′ endo sugar puckers, the shape of the duplex is very much like that of A-form DNA. Thus, although the bend angles and platinum displacements from the guanine planes differ, the major effects of helix unwinding and minor groove opening are quite similar in nature. This shape similarity between the solution and crystal structures is further illustrated in Figure 6C. The view in this figure superimposes the first

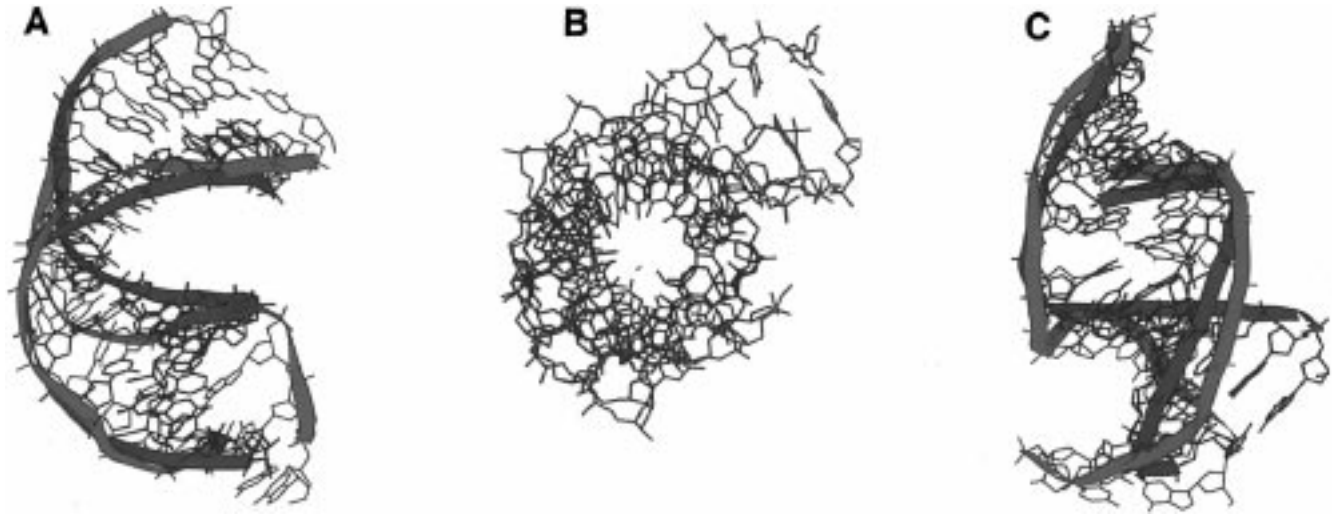

FIGURE 6: The structures of the NMR solution (shown in red) and X-ray crystal (shown in blue) structures superimposed over the first 8 base pairs. (A) The side view shows the similarity in bend angle and curvature over the 5′ end of the structures. (B) A view down the helix axis from the 5′ end showing the hole down the center of the duplex similar to that observed in A-form DNA. (C) A view from the minor groove opposite the Pt atom. The ribbon trace of the sugar−phosphate backbone show the similarity of the minor groove width and global curve over the first 8 base pairs of the two structures.

eight base pairs. The minor grooves are depicted as ribbons used to trace the sugar−phosphate backbone. It is especially evident in this view that the two structures differ most in the global deformation of the helix toward the 3′ end.

Table 2 compiles selected structural features of the crystal and solution structures of the cisplatin modified duplexes **1** and **2** just discussed and includes for comparison results for the DNA in complexes with hSRY (*23*) and LEF-1 (*24*). These and other HMG-domain proteins form specific complexes with DNA containing *cis*-diammineplatinum(II) 1,2-intrastrand d(GpG) cross-links (*6*, *8*, *9*), which can modulate the biological activity of cisplatin (*12*). Gel electrophoresis studies (*35*) have indicated that the binding of HMG domains to cisplatin-damaged DNA induces further bending of the duplex. This observation is consistent with DNA geometric deformations observed in the LEF-1/DNA (*24*) and hSRY/DNA (*23*) solution structures.

The ability of the *cis*-$\{Pt(NH_3)_2\}^{2+}$ cross-link to effect a global structure modification of DNA is probably due to roll induced at the G*pG* step. The accompanying bend of the helix and widening of the minor groove afford a geometry which facilitates recognition of platinated DNA by the HMG-domain family of proteins. In the LEF-1 structure, the 15 base pair DNA is bent by nearly 117° (*24*), and in the hSRY complex, the octameric DNA bends by 70−80° (*23*). In both cases, the duplexes are severely distorted with a widened and flattened minor groove and helix unwinding localized near the center of the bend. These global deformations resemble the major structural features observed for duplex **1**.

In the structure of the LEF-1 complex, a methionine residue from the HMG domain intercalates between adjacent adenosine bases A23 and A24 in the sequence d(C_1A_2-$C_3C_4C_5T_6T_7T_8G_9A_{10}A_{11}G_{12}C_{13}T_{14}C_{15}$)·d($G_{16}A_{17}G_{18}C_{19}T_{20}T_{21}$-$C_{22}A_{23}A_{24}A_{25}G_{26}G_{27}G_{28}T_{29}G_{30}$), bending the DNA toward the major groove. The roll between these adenosine residues is similar to that between adjacent guanosines in **1** (*17*). Superposition of the solution structure of **1** over the 12 central base pairs, running from A2/T29 through C13/G18, of the

FIGURE 7: A view into the minor groove of the superposition of the solution structure of the duplex **1** (shown in red) and the central 12 base pairs (A2/C29 to C13/G18) of the DNA from the LEF-1 complex (shown in blue). The shape of the minor grooves and global deformation of the helix axis are very similar in these two models.

LEF-1 DNA revealed that the best fit was obtained when the T7/T8 bases of the latter were overlaid on the platinated guanosines comprising the 1,2-intrastrand cross-link. The result of such a superposition is shown in Figure 7. The overlap is quite good with an RMSD of 3.2 Å for the sugar−phosphate backbone of the 12 base pairs. It is evident from a view into the minor groove of these duplexes (Figure 7) that the distortion caused by cisplatin is very similar to that brought about by binding of the transcription factor LEF-1 to its recognition sequence. Although a significant bend in duplex DNA like that in **1** is often accompanied by an intermolecular interaction with a protein or end of another DNA molecule as occurs in the crystal structure (*16*, *17*),

there is no NMR experimental evidence for such a contact here.

The comparison with the LEF-1 complex provides a structural rationale for the ability of cisplatin-modified DNA to serve as a recognition signal for binding HMG-domain proteins. Such an interaction modifies the toxicity of cisplatin in yeast and blocks excision repair in human cell extracts (*7*). HMG-domain proteins bind to their recognition sequences in the minor groove. Platinum binding to adjacent purine N7 atoms causes significant unwinding of the helix and bending toward the major groove, allowing the minor groove to be opened up and leading to recognition by the HMG-domains. Further details of this interaction will have to await the results of structural studies of complexes between an HMG domain and cisplatin-modified DNA, which are currently in progress.

ACKNOWLEDGMENT

We thank Dr. C. J. Turner from the Francis Bitter Magnet Laboratory for help with data collection, Dr. P. M. Takahara for valuable discussions, and Johnson Matthey AESAR/Alfa Co. for a gift of cisplatin.

SUPPORTING INFORMATION AVAILABLE

Figures S1−S6 containing the contour plots of the H8/H6-to-H2′/H2″, imino, amino-imino, aromatic, and H1′-to-H2′/H2″ regions of the 2D NOESY spectrum of **1**, a plot of roll versus base displacement, and Tables S1 and S2 containing torsion angles and helical parameters (9 pages). Coordinates of the final refined structure have been deposited in the Brookhaven Protein Database, acquistion number (1A84). Ordering information is given on any current masthead page.

REFERENCES

1. Fichtinger-Schepman, A. M. J., van der Veer, J. L., den Hartog, J. H. J., Lohman, P. H. M., and Reedijk, J. (1985) *Biochemistry 24*, 707−713.
2. Eastman, A. (1986) *Biochemistry 25*, 3912−3919.
3. Bellon, S. F., and Lippard, S. J. (1990) *J. Biophys. Chem. 35*, 179−188.
4. Bellon, S. F., Coleman, J. H., and Lippard, S. J. (1991) *Biochemistry 30*, 8026−8035.
5. Reed, E., Ozols, R. F., Tarone, R., Yuspa, S. H., and Poirier, M. C. (1987) *Proc. Natl. Acad. Sci. U.S.A. 84*, 5024−5028.
6. Chow, C. S., Barnes, C. M., and Lippard, S. J. (1995) *Biochemistry 33*, 2954−2964.
7. Whitehead, J. P., and Lippard, S. J. (1996) in *Metal Ions in Biological Systems* (Sigel, A., and Sigel, H., Eds.) pp 687−725, Marcel Dekker, Inc, New York.
8. Ohndorf, U.-T., Whitehead, J. P., Raju, N. L., and Lippard, S. J. (1997) *Biochemisry 36*, 14807−14815.
9. Trimmer, E. E., Zamble, D. B., Lippard, S. J., and Essigmann, J. M. (1998) *Biochemistry 37*, 352−362.
10. Huang, J.-C., Zamble, D. B., Reardon, J. T., Lippard, S. J., and Sancar, A. (1994) *Proc. Natl. Acad. Sci. U.S.A. 91*, 10394−10398.
11. Zamble, D. B., Mu, D., Reardon, J. T., Sancar, A., and Lippard, S. J. (1996) *Biochemistry 35*, 10004−10013.
12. McA'Nulty, M. M., Whitehead, J. P., and Lippard, S. J. (1996) *Biochemistry 35*, 6089−6099.
13. Sherman, S. E., Gibson, D., Wang, A. H.-J., and Lippard, S. J. (1985) *Science 230*, 412−417.
14. Sherman, S. E., Gibson, D., Wang, A. H.-J., and Lippard, S. J. (1988) *J. Am. Chem. Soc. 110*, 7368−7381.
15. Dunham, S. U., and Lippard, S. J. (1995) *J. Am. Chem. Soc. 117*, 10702−10712.
16. Takahara, P. M., Rosenzweig, A. C., Frederick, C. A., and Lippard, S. J. (1995) *Nature 377*, 649−652.
17. Takahara, P. M., Frederick, C. A., and Lippard, S. J. (1996) *J. Am. Chem. Soc 118*, 12309−12321.
18. Huang, H., Zhu, L., Reid, B. R., Drobny, G. P., and Hopkins, P. B. (1995) *Science 270*, 1842−1845.
19. Paquet, F., Perez, C., Leng, M., Lancelot, G., and Malinge, J.-M. (1996) *J. Biomol. Struct. Dyn. 14*, 67−77.
20. den Hartog, J. H. J., Altona, C., van Boom, J. H., van der Marel, G. A., Haasnoot, C. A. G., and Reedijk, J. (1985) *J. Biomol. Struct. Dynam. 2*, 1137−1154.
21. Herman, F., Kozelka, J., Stoven, V., Guittet, E., Girault, J.-P., Huynh-Dinh, T., Igolen, J., Lallemand, J.-Y., and Chottard, J.-C. (1990) *Eur. J. Biochem. 194*, 119−133.
22. Yang, D., van Boom, S. S. G. E., Reedijk, J., van Boom, J. H., and Wang, A. H.-J. (1995) *Biochemistry 34*, 12912−12921.
23. Werner, M. H., Huth, J. R., Gronenborn, A. M., and Clore, G. M. (1995) *Cell 81*, 705−714.
24. Love, J. J., Li, X., Case, D. A., Giese, K., Grosschedl, R., and Wright, P. E. (1995) *Nature 365*, 791−795.
25. Brünger, A. T. (1992) *X-PLOR Version 3.1. A System for X-ray Crystallography and NMR*, Yale University Press, New Haven, CT.
26. Wuthrich, K. (1986) *NMR of Proteins and Nucleic Acids*, John Wiley & Sons, New York.
27. Wijmenga, S. S., Mooren, M. M. W., and Hilbers, C. W. (1993) in *NMR of Macromolecules, A Practical Approach* (Roberts, G. C. K., Ed.) pp 217−288, Oxford University Press, New York.
28. Nilges, M., Habazettl, J., Brünger, A. T., and Holak, T. A. (1991) *J. Mol. Biol. 219*, 499−510.
29. Yip, P., and Case, D. A. (1989) *J. Magn. Reson. 83*, 643−648.
30. Lavery, R., and Sklenar, H. (1988) *J. Biomol. Struct. Dyn. 6*, 63−91.
31. Lavery, R., and Sklenar, H. (1989) *J. Biomol. Struct. Dyn. 6*, 655−674.
32. Dickerson, R. E. (1989) *J. Biomol. Struct. Dyn. 6*, 627−640.
33. Dunham, S. U., Dunham, S. U., Turner, C. J., and Lippard, S. J. (1998) *J. Am. Chem. Soc.* (In press).
34. Saenger, W. (1984) *Principles of Nucleic Acid Structure*, Vol. 1, 1st ed., Springer-Verlag, New York.
35. Chow, C. S., Whitehead, J. P., and Lippard, S. J. (1994) *Biochemistry 33*, 15124−15130.
36. Kraulis, P. J. (1991) *J. Appl. Crystallogr. 24*, 946−950.

BI973176V